Title

Predicting Aerosol Reactivity Across Scales: from the Laboratory to the Atmosphere

Journal

Environmental Science and Technology, 52(23)

ISSN

0013-936X

Authors

Houle, Frances A

Wiegel, Aaron A

Wilson, Kevin R

Publication Date

2018-12-04

DOI

10.1021/acs.est.8b04688

Peer reviewed

Predicting aerosol reactivity across scales: from the laboratory to the atmosphere

Frances A. Houle, Aaron A. Wiegel and Kevin R. Wilson**

Chemical Sciences Division, Lawrence Berkeley National Laboratory, 1 Cyclotron Road, Berkeley, CA 94720

ABSTRACT

To fully utilize the results of laboratory-based studies of the chemistry of model atmospheric aerosol reactions, it is important to understand how to relate them to the conditions found in nature. In this study, we have taken a validated reaction-diffusion mechanism for oxidation of $C_{30}H_{62}$ aerosol by OH under flow tube conditions and examined its predictions for another experimental regime (continuous flow stirred tank reactor) and for the atmosphere, spanning alkane aerosol viscosities from liquid to semi-solid. The results show that under OH-concentration-limited and aerosol-mixing-limited conditions, it should be possible to select laboratory experimental conditions where many aspects of the particle phase and volatile product chemistry under atmospheric conditions can be revealed. If the OH collision and organic diffusion rates are comparable, however, reactivity is highly sensitive to the details of both OH concentration and internal mixing. The characteristics of the transition between limiting

conditions provide key insights into which parts of the reaction mechanism dominate in the various kinetic regimes.

Introduction

Laboratory studies are central for interpreting field observations and parameterizing models to understand and ultimately predict chemical transformations in the atmosphere.[1] Gas-phase rate coefficients, yields and formation mechanisms of secondary organic aerosol, and multiphase transformation mechanisms and rates provide quantitative parameters needed to improve the fidelity of regional and climate models. A key challenge, noted by many, is developing reliable methods to mimic or reliably extrapolate the chemistry conducted in the laboratory-scale reactors to the real atmosphere.[2-7] Central to this challenge is the difficulty of matching laboratory and atmospheric concentrations and timescales that often differ by orders of magnitude.

To determine the oxidation lifetime of many trace gas species, rate coefficients can be easily quantified under laboratory conditions and directly applied to atmospheric conditions. Here the experimental challenge centers on understanding complex reaction networks and accurately providing oxidation conditions and trace gas levels to reproduce the competition between bimolecular and unimolecular pathways in polluted and pristine regions of the atmosphere. This is nicely illustrated by the recent discovery of the importance of unimolecular autoxidation pathways[8, 9] of gas-phase peroxy radicals (RO_2) when bimolecular reactions of NO are suppressed (e.g. a source of aerosol in the pristine regions of the atmosphere[10-12]). Another example is the formation and chain propagation of aerosol-phase alkoxy radicals when reaction

conditions are designed to favor RO_2 + NO or SO_2 (i.e., the urban atmosphere) rather than typical laboratory oxidation conditions that naturally favor RO_2 + RO_2 pathways.[13, 14]

It is not so straightforward, however, to examine the coupling of gas-aerosol interactions with oxidative ageing of aerosols. Direct extrapolation of laboratory observations to the atmosphere becomes more tenuous due to the emergence of additional timescales (i.e., particle-phase diffusion, uptake, evaporation) within the aerosol particles that can govern the kinetics. For example, heterogeneous oxidation lifetimes (involving OH or O_3) and oxidized product distributions of organic species in aerosol are not determined solely by intrinsic reactivity but are often complex, time-dependent functions of internal aerosol mixing timescales.[15-22] This is because when internal mixing is slow (e.g., a semisolid), reactions are localized at the aerosol surface, while rapid mixing in liquids results in uniform composition changes and scaling of overall reactivity with particle volume. Whether a reaction is localized to a surface or scales with volume does not depend on aerosol viscosity alone, but is an emergent property[18] that depends upon oxidant concentration in the gas phase and particle diameter. What is most important is the time between oxidant collisions with the particle surface relative to the mixing time within the aerosol. Thus, in the laboratory, reactions using semisolid aerosol at high [OH] and short reaction times may not replicate the heterogeneous chemistry occurring over the long time, low oxidant field of the atmosphere. A semisolid aerosol in the laboratory may in fact appear well-mixed in the atmosphere since aerosol constituents have ample time to sample the entire particle volume between reactive events. New approaches are needed to better understand when the results of existing laboratory experiments can be extrapolated to other conditions, and

to guide the design of experiments that more faithfully replicate the coupling of diffusive and reactive timescales of the atmosphere.

In the present work, we report results of a comprehensive computational study that provides a means to connect laboratory data to atmospheric aerosol chemistry using a single reaction-diffusion mechanism that has been validated for liquid and semisolid alkane aerosol oxidation.[22, 23] It builds on an initial investigation in which we predicted the compositions of 200 nm diameter aerosol particles with a range of viscosities intermediate between liquid and solid for an OH partial pressure typical of laboratory flow tube conditions ([OH] = 5.04 x 10^{10} molec./cm^3).[19] We introduced a reaction-diffusion index (I_{RD}) to provide a quantitative link between particle viscosity and reactivity, enabling identification of the specific parts of the free radical chain reaction mechanism that dominate aerosol composition when the relative extent of mixing is varied. Here, we use the same reaction scheme to predict both aerosol and volatile product compositions as well as aerosol size and mass under OH densities typical of flow tube (FT, [OH] = 5.04 × 10^{10} molec./cm^3) and continuous flow stirred tank[24] (CFSTR, [OH] = 5.04 × 10^8 molec./cm^3) reactors and the atmosphere ([OH] = 5.04 × 10^6 molec./cm^3). The results are analyzed in terms of I_{RD}, allowing identification of regimes where atmospheric reactivity of alkanes is readily predictable from laboratory experiments, and where it is not. The simulations provide insights to how product distributions, regimes, and factors that control the kinetics are connected.

Simulations

4

The free radical oxidation scheme used in this work was developed and validated for reaction between OH and $C_{30}H_{62}$ in liquid (squalene) and semisolid (triacontane) under laboratory flow tube conditions.[22, 23] The chain reaction is launched by H abstraction from the alkane, forming alkyl radicals that rapidly condense with available O_2 to form peroxy radicals. O_2 is assumed to be instantly replenished from the surrounding gas due to its fast diffusion through liquids and solid organics.[25, 26] The peroxy radicals disproportionate and fragment through subsequent chain reactions, forming a variety of condensed and gas - phase products. A summary of the reaction scheme is presented in the Supporting Information (SI), Section 1. Since known or calculated rate constants are used for the elementary reaction steps involved, rather than adjustable parameters, and the mechanism spans initial abstraction to fully oxidized CO_2, the simulations are predictive for a broad range of reaction conditions even outside of those used to establish the reaction scheme.

In the description we have developed for the free radical reactions involved in alkane oxidation,[23] the individual product molecules formed by free radical functionalization and fragmentation reactions are not explicitly included. Rather, molecules are represented as a set of functionalities and carbon backbone lengths to allow the essential characteristics of the chemical system to be captured, while minimizing the extreme complexity of tracking all the kinds of molecules that can be generated by a free radical chain spanning H abstraction from pure hydrocarbon to formation and evaporation of CO_2. The initial $C_{30}H_{62}$ molecule is taken to be a straight chain with primary and secondary alkyl groups for all aerosol viscosities, thus neglecting the branching that adds tertiary carbon reactions[23] and reduces viscosity.[27] The free radical groups generated during the reaction are alkyl, peroxy, alkoxy, acyl, acyl peroxy and acyloxy,

5

located at primary or secondary positions. The radicals react further to form ketone, aldehyde, carboxylic acid and alcohol functionalities, accompanied by C_{30} chain fragmentation. Stochastic reaction-diffusion simulation methods[23] have been used to perform simulations using this scheme to generate spatially resolved concentration *vs* time curves that include the effect of variable volume on instantaneous rates. The software package is Kinetiscope.[28] The 200-nm-diameter aerosol is represented by an array of 200 13.17 nm × 13.17 nm × 0.5 nm compartments located along the particle radius when full reaction-diffusion simulations are performed, or by a single compartment when the diffusion coefficient is fast enough for the particle to be well-mixed at all times.

In our initial study assuming FT conditions,[19] the $C_{30}H_{62}$ diffusion coefficients were varied from 1 x 10^{-11} (liquid) to 8.39 × 10^{-19} cm^2/s (semi-solid using the diffusion coefficient of triacontane derived from viscosity measurements[29]) in increments of factors of 10, and all product species in the simulation were assumed to diffuse with the same coefficient as the initial alkane throughout the system, neglecting possible decreases in viscosity as the particle composition changes. This range is typical of self-diffusion in semisolid α-pinene SOA.[30] In this paper, we use this scheme to predict both gas and condensed phase products for the same viscosity range over a broad OH concentration range, representing FT, CFSTR and atmospheric conditions. Table 1 lists the OH densities studied, with reaction times selected to reach a constant total OH exposure of 3.024 × 10^{12} molecules cm^{-3} s. The largest diffusion coefficients used for fully spatially resolved FT, CFSTR, and atmospheric reaction-diffusion simulations are 10^{-11}, 10^{-13}, and 10^{-15} cm^2/s, respectively. Above these values, the aerosol is well-mixed and the calculations become very expensive. Instead, we can represent the system accurately by single

6

compartment simulations with instantaneous mixing as shown in Houle et al[18] and Wiegel et al.[22, 23]

Table 1. Simulation conditions for OH + $C_{30}H_{62}$

Conditions	OH concentration molec/cm^3	Reaction time (s)	Self-diffusion coefficients (cm^2/s)	OH Exposure (molec. cm^{-3} s)
Laboratory flow tube (FT)[a]	5.04×10^{10} (31, 32)	60	instantaneous, $10^{-11} - 8.39 \times 10^{-19}$	3.024×10^{12}
Continuous flow stirred tank (CFSTR)	5.04×10^{8} (24,13, 14)	6000	instantaneous, $10^{-13} - 8.39 \times 10^{-19}$	3.024×10^{12}
Atmosphere, daytime	5×10^{6} (33,34)	604800 (1 week)	instantaneous, $10^{-15} - 8.39 \times 10^{-19}$	3.024×10^{12}

a. Simulation results for FT conditions are taken from Houle et al.[19]

7

Results

The simulations provide complete data sets for volume, mass, carbon chain lengths and functionality concentrations in the particle and gas phases as a function of time. Spatial distributions of all particle-phase species are generated when a multicompartment scheme is used. These results are analyzed to compare the outcomes of the oxidation reaction over a broad range of conditions, providing new information on how reactivity varies with OH concentration and aerosol viscosity. Details of the simulated data are presented in the SI, Section 2.

I. Trends in consumption of $C_{30}H_{62}$ by OH reactions

A striking result of the simulations is the emergence of distinctive patterns in several particle properties as viscosity and OH concentration are varied. For example, nearly identical $C_{30}H_{62}$ decay curves (Figure S1) and spatial distributions (Figure S2) as a function of time are found for FT, CFSTR and atmospheric OH densities when diffusion coefficients are offset by about 2 orders of magnitude. These self-similarity trends are surprising but can be rationalized by considering the relative rates of reaction and internal mixing via self-diffusion, which controls the concentration of abstractable hydrogen near the aerosol surface where most reactions with OH take place.[18, 35] As described previously,[19] a reaction-diffusion index, I_{RD} can be defined as:

$$I_{RD} = \frac{k_{rxn}\left[\mathrm{OH(g)}\right] d_p^2}{4\pi^2 D} \quad (1)$$

where k_{rxn} is the rate constant for reaction between OH and species in the particle, d_p is the particle diameter, [OH(g)] is the concentration of OH in the gas phase and D is the self-diffusion

coefficient of organic molecules in the particle. When important characteristics of the reactions such as initial uptake

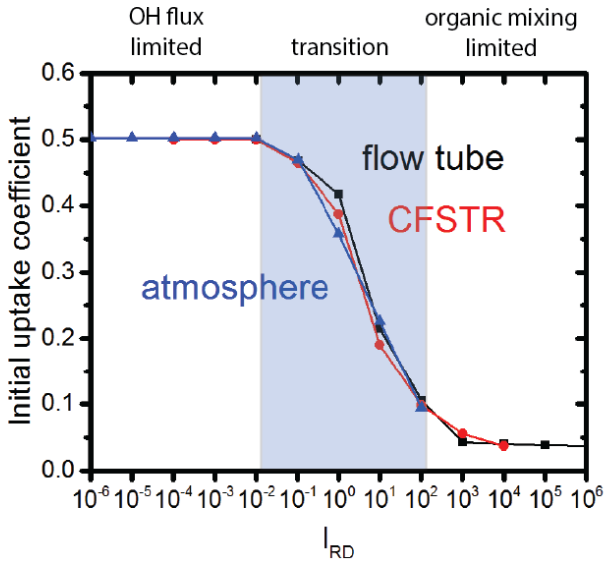

Figure 1. Initial uptake coefficients for $C_{30}H_{62}$ reacting with all three OH concentrations as a function of I_{RD}. The IRD ranges corresponding to the limiting kinetic regimes are labeled.

coefficients and ratios of products as a function of OH concentration and *D* are plotted as a function of I_{RD}, trends are captured in a way that allows these characteristics to be compared self-consistently. As shown in Figure 1, initial uptake coefficients calculated from the decay curves in Figure S1 are nearly coincident, indicating that at the very early stages of oxidation, the kinetic factors that control $C_{30}H_{62}$ consumption are essentially unchanged over a 10^4 variation in OH concentration. Table S1 lists the values for I_{RD} for each combination of diffusion coefficient and OH concentration used in Figure 1.

9

The definition of I_{RD} is closely related to the definition of the uptake coefficient, γ, through the reacto-diffusion length, L.[18] If the aerosol is well-mixed, $2L$ is equal to the diameter of the particle. If it is not, $d_p > 2L$, and the more general expression for γ is

$$\gamma = \frac{2 k_{rxn} \rho_0 N_A}{3 c M d_p^2} \left[d_p^3 - \left(d_p - 2L \right)^3 \right] \quad (2)$$

where ρ_0 is the aerosol density, c is the velocity of the OH molecules, M is the molecular weight of the aerosol material, and N_A is Avogadro's number. Specifically,[18]

$$L = \left(\frac{2 k_{rxn}}{I_{RD} \pi^3 c \sigma} \right)^{1/2} \quad (3)$$

where σ is the probability that a colliding OH will stick to the aerosol surface long enough to react.

As I_{RD} increases due to decreasing D (increasing viscosity) and/or increasing OH gas concentration, both L and γ decrease. This trend is evident in Figure 1, where all three γ vs I_{RD} datasets fall on a single curve, with 3 distinct regimes. When $I_{RD} < 10^{-2}$, γ is essentially constant at a value similar to that for OH reaction with liquid squalane under FT conditions,[36] and reflects reactivity controlled only by OH reactions at the aerosol surface. When $I_{RD} > 10^{2}$, γ is similarly constant, but with a value lower than reported in previous work.[13, 37] However, a quantitative comparison of the predicted and experimental values for γ is complicated by the fact that the decay curves used to calculate γ are not exponential and the experimental particle geometry is not well-defined. The OH concentration- and organic-mixing-limited cases are separated by a transition region where γ decreases rapidly.

II. Trends in physical properties

10

Although the uptake coefficients follow a regular pattern, other characteristics do not. Aerosol final diameters and masses are compared in Figure 2, and masses as a function of time for the 3 OH densities are shown in Figure S3. The variation in final diameter with I_{RD} is not monotonic: it passes through a minimum around I_{RD} =10-100, which coincides with the uptake coefficient transition regime shown in Figure 1. The final particle mass, on the other hand, decreases as I_{RD} increases. Under well-mixed conditions when $I_{RD} < 10^{-2}$, there is a net mass

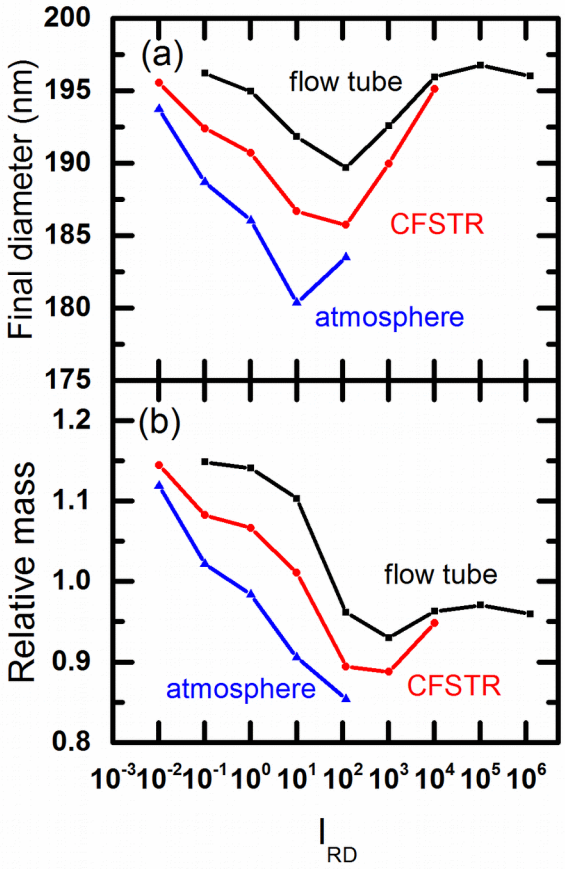

Figure 2. Aerosol diameter and mass characteristics after OH exposure. The mass is relative to the initial mass of unreacted $C_{30}H_{62}$.

11

increase relative to the pure alkane due to oxygen incorporation. The mass increase competes with mass loss due to fragmentation and volatilization as the diffusion coefficient decreases and the chemistry becomes self-diffusion limited. The extent of mass loss increases with decreasing gas - phase OH concentration, and is most pronounced under atmospheric conditions, where OH concentration is lowest. This result indicates that there are significant differences in reactivity as OH concentration and particle viscosity are varied even though the reaction mechanism is the same.

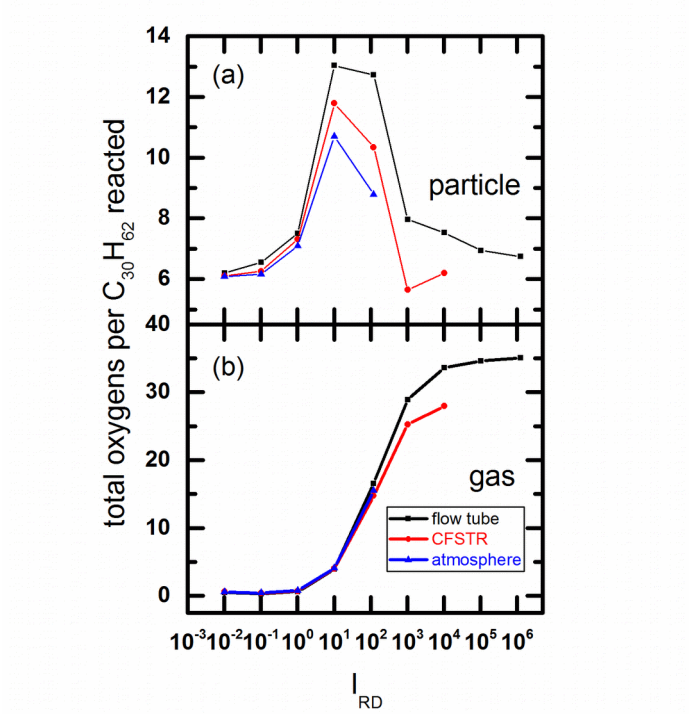

Figure 3. Total functional groups present (a) in the aerosol particle and (b) in the gas phase (including CO_2) after OH exposure, normalized to the total amount of $C_{30}H_{62}$ reacted, for the three OH densities.

III Trends in particle and gas - phase oxidation products

12

The simulations track the functionalities formed during oxidation in both the condensed and gas phases. Figure 3 shows the total accumulated oxygen-containing functionalities in the particle and gas phases per $C_{30}H_{62}$ reacted, which reflects the extent of reaction over the range of OH densities and viscosities. Figure 3a shows that functionality accumulation in the particle is similar for all OH densities when mixing is fast, increases significantly in the I_{RD} transition region, then decreases as the reaction becomes mixing limited. Figure 3b shows that this trend is accompanied by very low fragmentation and volatilization to form oxidized gas products when mixing is fast transitioning to abundant gas product formation as I_{RD} increases into the mixing-limited regime.

Plots of the total amounts of each stable functionality as a function of time – ketones, alcohols, aldehydes, carboxylic acids and CO_2 – normalized to the instantaneous amount of unreacted $C_{30}H_{62}$ are presented in Figures S4-S12, organized according to I_{RD}. The data show that while the functionality compositions of the aerosol particles are similar for each I_{RD} across the full range of OH densities, those of the volatilized gases are not. Figures 4 and 5 summarize these results for the transition regime, showing the final functionality distributions corresponding to the totals in Figure 3 for particles and gas phase, respectively.

13

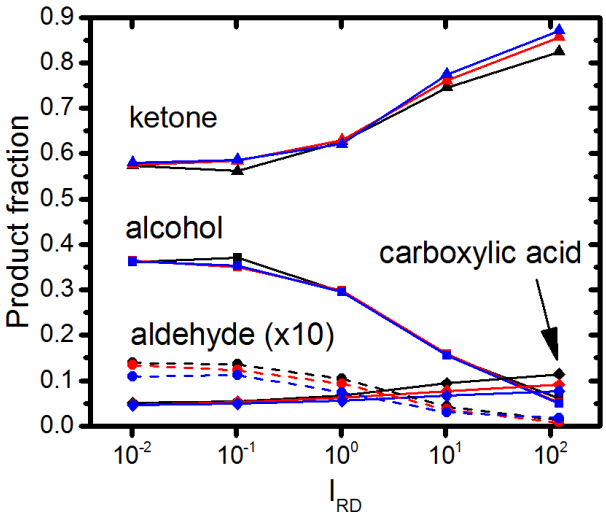

227

228

229**Figure 4.** Composition of aerosol particles after exposure to OH in the transition kinetic regime

230between [OH] limited and self-diffusion limited.

231

232

14

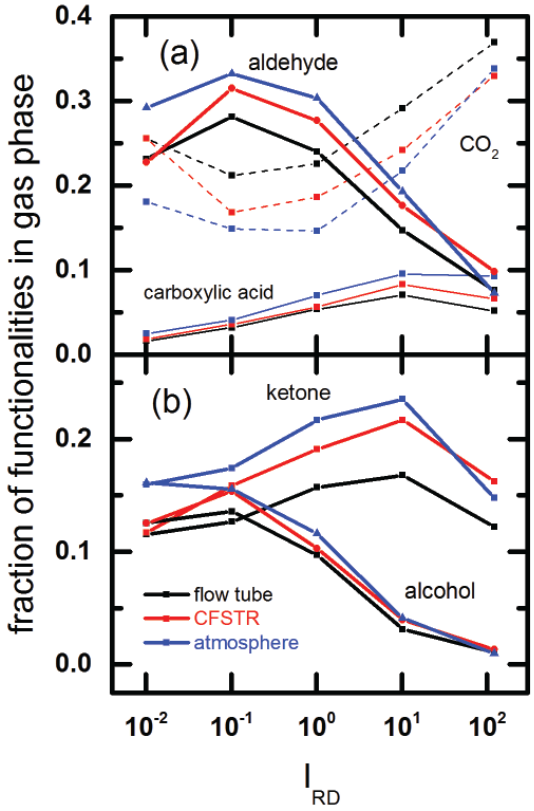

Figure 5. Composition of the gas phase surrounding the aerosol particles after exposure to OH in the transition kinetic regime between [OH] limited and self-diffusion limited. (a) gas products that originate from minority functionality components in the aerosol; (b) gas products that originate from majority functionality components in the aerosol.

The simulation results in Figure 4 show that there is a dramatic change in composition as a function of I_{RD} in the transition regime, with FT, CFSTR and atmospheric OH densities having the same chemistry although the extents of oxidation are quite different (Figure 3). Ketones become the dominant functional group, accompanied by a modest increase in carboxylic acids. The ketones are relatively unreactive to OH and accumulate as the reaction becomes self-diffusion-limited, unlike the alcohols which undergo a significant decrease in concentration. The

15

aldehydes, present in small amounts, also decrease with increasing I_{RD}. Carboxylic acids, although minor products, accumulate as the reaction becomes mixing limited.

The gaseous product distribution is qualitatively different from the particle phase composition, as shown in Figure 5. Although ketones and alcohols are the major particle phase components of the aerosol, aldehydes and CO_2 are the major volatile products. The OH concentration conditions affect the gas composition for two of the products: FT conditions, which have the highest OH-aerosol collision frequency, favor CO_2 volatilization, while atmospheric conditions favor ketone volatilization.

Inspection of the molecular chain lengths (carbon numbers) at I_{RD} =10 for the three OH regimes (Figure S13) shows that although the aerosol particle functionality distributions are very similar for the three OH concentration cases in the transition regime (Figure 4), the carbon numbers are not. As the OH concentration decreases from FT to atmosphere, the average carbon number at the end of OH exposure increases. Figure 2 shows that the particle mass decreases, however, with mass loss being greatest for the lowest OH concentration when I_{RD} =10. These results together with the data in Figures 3a, 5 and S7 show that under atmospheric concentrations, volatilization of oxidized functionalities is favored relative to FT conditions.

Discussion

Using a detailed reaction-diffusion mechanism developed and validated for the reaction of OH + semisolid and liquid $C_{30}H_{62}$ under FT conditions,[19, 23, 29] we have performed a computational study to predict oxidative aging chemistry for the much lower OH partial pressures typical of laboratory CFSTR and atmospheric conditions over a broad range of alkane

viscosities. Strong patterns in chemical and physical properties are evident as OH concentration and alkane self-diffusion coefficients are varied over ranges of 4 and 7 orders of magnitude, respectively. These patterns are rationalized in terms of the reaction-diffusion index I_{RD}, which is a measure of the balance between the availability of OH from the gas phase for H abstraction reactions and the extent of mixing by self-diffusion in the aerosol, for each combination of OH concentration and particle viscosity.

The results in Figures 4, and S4-S6 suggest that laboratory measurements of alkane aerosol particle compositions during reactions with OH under both FT and CFSTR conditions may be predictive of compositions under atmospheric conditions when the chemistry is strongly limited by arrival of OH at the aerosol surface ($I_{RD} < 10$). When $I_{RD} > 10$, the aerosol compositions are qualitatively similar, but not identical (Figures 4 and S7-S8). These trends continue into the higher I_{RD} range. The results in Figures 5 and S4-S12 show clearly that laboratory measurements will only be qualitatively predictive for the limiting cases and not predictive at all in the transition regime. Experimental tests of these findings will be very valuable for model validation and improvement, particularly measurements of particle size in the transition regime, and of the ratio of ketones to alcohols in the particle phase across the I_{RD} range.

To understand these trends, we examine the free radical oxidation chemistry involved in the three kinetic regimes, which is sketched in Figure 6. When the oxidation kinetics are in the OH concentration-limited range, the aerosol is relatively C-H rich. Abstraction events generate peroxy radicals, which form ketones and alcohols as the primary oxidation products for the OH exposure times studied. This simple picture only applies when internal mixing is fast and oxidized moieties are dilute. As the rates of OH reaction and self-diffusion become competitive,

the *sec*-peroxy radical concentration increases from near-zero to significant amounts and the reaction becomes confined to the near-surface region of the aerosol, as shown in Figures S2, S14 and S15.

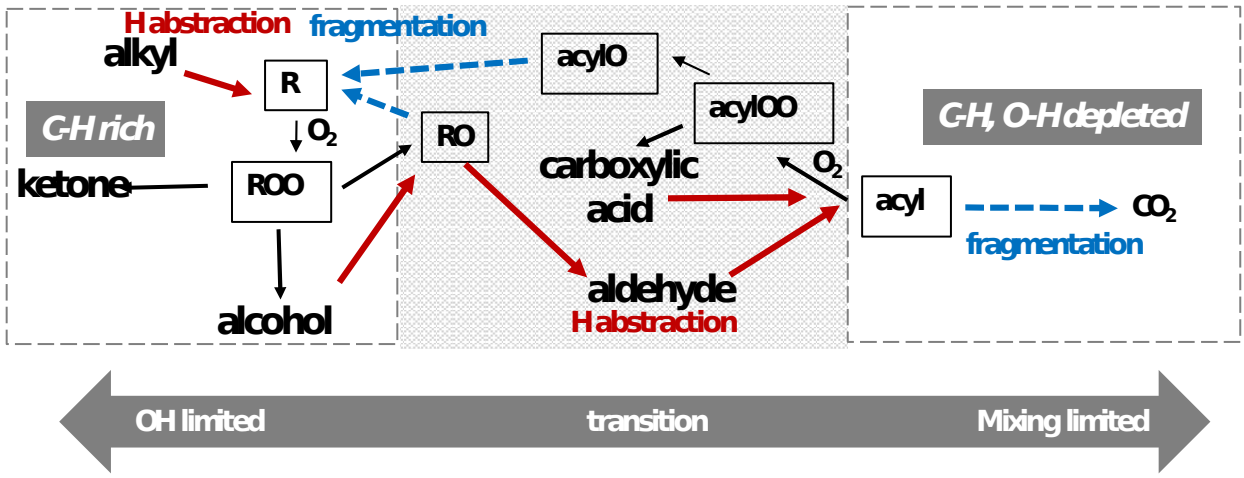

Figure 6. Abstraction, propagation, and product formation steps for the heterogeneous reaction of OH with alkanes. The blue arrows mark steps that are second order in peroxy radical concentration. Acyloxy and alkoxy radicals undergo unimolecular decomposition reactions and generate additional peroxy radicals. Under reaction-limited conditions (dashed line box), ketone and alcohol formation dominate. Under mixing limited conditions, the entire free radical chain is active.

The other radicals, which are more reactive, are present in negligible quantities. Under these conditions, disproportionation of peroxy radicals to form alkoxy radicals and O_2, which is quite slow when the aerosol is well-mixed,[18] becomes kinetically significant. Alkoxy radicals

18

fragment to form aldehydes and primary alkyl radicals that react and dissociate to form mixture of alkyl, peroxy, acyl, acyloxy and acylperoxy radicals. This intensely reacting environment rapidly consumes available C-H and O-H bonds, and the steady state population of peroxy radicals decreases to near-zero. These conditions favor acyl radical formation and fragmentation to form CO_2.

The chemical trends for alkane oxidation shown in Figure 6 connect the reaction mechanism to the product functionality distributions shown in Figures S4-S12. When $I_{RD} < 1$, particle phase ketones and alcohols dominate for all OH densities, with very little fragmentation to form volatiles, indicating that the chemistry does not go deeply into the free radical chain. This I_{RD} range corresponds to $D > 10^{-12}$ cm^2/s for FT conditions, $D > 10^{-14}$ cm^2/s for CFSTR conditions, and $D > 10^{-16}$ cm^2/s for atmospheric conditions for this particle size (200 nm initially). This suggests that FT measurements with liquid phase aerosol can be informative for atmospheric conditions even when the target atmospheric material is quite viscous. When $I_{RD} > 10^2$, the product distribution is also simple, dominated by ketones in the particle phase and CO_2 in the gas phase, consistent with formation of terminal products. The self-diffusion coefficient range for this regime is in the highly viscous fluid to semisolid range: $D > 10^{-14}$ cm^2/s for FT conditions, $D > 10^{-16}$ cm^2/s for CFSTR conditions, and $D > 10^{-18}$ cm^2/s for atmospheric conditions for 200 nm particles. Given the challenges of generating well-controlled solid aerosol nanoparticles, laboratory investigations of the oxidation of highly viscous liquids may be a reasonable proxy to learn about reactivity in the atmosphere. The correlation by I_{RD} allows development of similar useful experimental strategies for other particle diameters.

19

While the initial uptake coefficients and condensed phase functionality distributions are independent of OH concentration in the transition region, the gas product distribution, extent of fragmentation, particle mass and particle diameter are not, and it is not possible to extrapolate between the OH concentration ranges without use of explicit reaction-diffusion models. Moreover, some features appear only in this range. For example, as shown in Figure 3, there is a dramatic increase in formation of oxygen-containing functionalities in the particle and mass loss relative to the OH concentration and self-diffusion limited regimes, as well as an increase in peroxy radical densities. Examination of Figures S4-S12 reveals that the primary chemical signature of the transition region is the OH concentration-dependence of the relative amounts of gaseous products, specifically CO_2 relative to aldehydes. In addition, Figure S15 shows that peroxy radicals have a lower steady state concentration above I_{RD} =1 for CFSTR conditions relative to FT and atmosphere. This pattern reveals that the delicate balance between mixing and reaction mainly affects the formation and subsequent reactions of alkoxy radicals. Since aldehydes are formed via H abstraction from alcohols and subsequent fragmentation to form aldehydes and new peroxy radicals, this suggests that the peroxy radical disproportionation chemistry dominates under CFSTR conditions, reducing the peroxy radical population relative to higher and lower OH densities and generating volatile aldehydes. FT and atmospheric OH densities, on the other hand, favor acyl radical formation and fragmentation. Although OH concentration is lowest under atmospheric conditions, the extent of erosion of the aerosol is greatest in the transition region, leading to a change of about 20% in particle diameter. This indicates that fragmentation to form volatiles is favored when free radical chain initiation events are relatively rare, consistent with carbon numbers in Figure S13.

20

Previous investigations have also sought to develop predictive correlations for heterogeneous aerosol reactions using reaction- and diffusion-limited kinetic regimes.[15] In particular, low diffusion rates in semisolids have been proposed to lead to extended lifetimes for organics in the troposphere.[38-40] It has been suggested that aerosol becomes more viscous during aging, and hence less prone to degradation.[41] The broad trends investigated here for an alkane model system indicate that extrapolations across a range of [OH] and viscosity conditions may not be possible in any simple way depending on the details of the chemistry, reacting environment and particle sizes involved.

The combinations of chemical and physical factors that control lifetimes at various stages of aging remain to be fully identified, but are likely to involve the following elements. Important reactions introduced by the presence of alkenes include oligomerization and efficient free radical cycling via hydroxyalkyl chemistry.[42] While the presence of NO_2 can be neglected if the aerosol is relatively dry, heterogeneous NO reactions can accelerate the oxidation process. NO promotes free radical cycling and fragmentation by increasing the extent of formation of alkoxy radicals even under well-mixed conditions.[13] Uptake of gaseous water becomes important as the particle becomes more hydrophilic. Particle-phase water adds acid-base chemical pathways that can promote fragmentation[43] and can decrease viscosity as can chain fragmentation under dry conditions. Inclusion of all of these elements, which are very important to be able to describe aerosol aging correctly, can be done in a straightforward way by modifying the basic mechanistic framework used here, if sufficient experimental data are available to validate the calculations. We can anticipate some of the effects. As viscosities decrease, they will cause a decrease in the relevant I_{RD} (Eq 1), and may cause the system to enter a kinetic regime that is more gas-collision-

21

controlled. However, the effect of such a change on particle composition and properties would likely not be pronounced unless the change is from the mixing-limited to the transition regime or from the transition regime to the OH limited regime. While we compare 200 nm particles in all cases, the I_{RD} analysis allows experimental data obtained on one size of particle to be used to predict oxidation on a different size if there are no changes in the chemistry or viscosity. Extensions of the present work to include additional reactions and composition-dependent viscosities will be valuable for development of new generalizations of chemical transformations for atmospheric chemistry models.

ASSOCIATED CONTENT

Supporting Information. Summary of the OH oxidation mechanism. Detailed plots of simulation results including spatial maps and compositions as a function of time. This material is available free of charge via the Internet at http://pubs.acs.org.

AUTHOR INFORMATION

Corresponding Authors: *Email: fahoule@lbl.gov. Tel.: (510) 495-8135; Email: krwilson@lbl.gov, Tel.: (510) 495-2474.

ACKNOWLEDGMENT

The early development of the reaction mechanism and simulation runs was supported by the Laboratory Directed Research and Development program at Lawrence Berkeley National

Laboratory under U.S. Department of Energy Office of Science, Office of Basic Energy Sciences under Contract No. DE-AC02-05CH11231. Later analysis of the simulations results was supported by the Department of Energy, Office of Science, Office of Basic Energy Sciences, Chemical Sciences, Geosciences, and Biosciences Division, in the Gas Phase Chemical Physics Program under Contract No. DE-AC02-05CH11231. We are grateful to Dr. William D. Hinsberg (Columbia Hill Technical Consulting) for helpful discussions on simulation approaches during the course of this work.

23

REFERENCES

1. Burkholder, J. B.; Abbatt, J. P. D.; Barnes, I.; Roberts, J. M.; Melamed, M. L.; Ammann, M.; Bertram, A. K.; Cappa, C. D.; Carlton, A. G.; Carpenter, L. J.; Crowley, J. N.; Dubowski, Y.; George, C.; Heard, D. E.; Herrmann, H.; Keutsch, F. N.; Kroll, J. H.; McNeill, V. F.; Ng, N. L.; Nizkorodov, S. A.; Orlando, J. J.; Percival, C. J.; Picquet-Varrault, B.; Rudich, Y.; Seakins, P. W.; Surratt, J. D.; Tanimoto, H.; Thornton, J. A.; Tong, Z.; Tyndall, G. S.; Wahner, A.; Weschler, C. J.; Wilson, K. R.; Ziemann, P. J., The essential role for laboratory studies in atmospheric chemistry. *Environmental Science & Technology* **2017,** *51*, (5), 2519-2528.

2. Rudich, Y.; Donahue, N. M.; Mentel, T. F., Aging of organic aerosol: bridging the gap between laboratory and field studies. *Annual Review of Physical Chemistry* **2007,** *58*, (1), 321-352.

3. George, C.; Ammann, M.; D'Anna, B.; Donaldson, D. J.; Nizkorodov, S. A., Heterogeneous photochemistry in the atmosphere. *Chemical Reviews* **2015,** *115*, (10), 4218-4258.

4. Pöschl, U.; Shiraiwa, M., Multiphase chemistry at the atmosphere–biosphere interface influencing climate and public health in the anthropocene. *Chemical Reviews* **2015,** *115*, (10), 4440-4475.

5. Abbatt, J. P. D.; Lee, A. K. Y.; Thornton, J. A., Quantifying trace gas uptake to tropospheric aerosol: recent advances and remaining challenges. *Chemical Society reviews* **2012,** *41*, 6555-81.

6. Jimenez, J. L.; Canagaratna, M. R.; Donahue, N. M.; Prevot, A. S. H.; Zhang, Q.; Kroll, J. H.; DeCarlo, P. F.; Allan, J. D.; Coe, H.; Ng, N. L.; Aiken, A. C.; Docherty, K. S.; Ulbrich, I. M.; Grieshop, A. P.; Robinson, A. L.; Duplissy, J.; Smith, J. D.; Wilson, K. R.; Lanz, V. A.; Hueglin, C.; Sun, Y. L.; Tian, J.; Laaksonen, A.; Raatikainen, T.; Rautiainen, J.; Vaattovaara, P.; Ehn, M.; Kulmala, M.; Tomlinson, J. M.; Collins, D. R.; Cubison, M. J.; Dunlea, J.; Huffman, J. A.; Onasch, T. B.; Alfarra, M. R.; Williams, P. I.; Bower, K.; Kondo, Y.; Schneider, J.; Drewnick, F.; Borrmann, S.; Weimer, S.; Demerjian, K.; Salcedo, D.; Cottrell, L.; Griffin, R.; Takami, A.;

24

Miyoshi, T.; Hatakeyama, S.; Shimono, A.; Sun, J. Y.; Zhang, Y. M.; Dzepina, K.; Kimmel, J. R.; Sueper, D.; Jayne, J. T.; Herndon, S. C.; Trimborn, A. M.; Williams, L. R.; Wood, E. C.; Middlebrook, A. M.; Kolb, C. E.; Baltensperger, U.; Worsnop, D. R., Evolution of organic aerosols in the atmosphere. *Science* **2009,** *326*, 1525-1529.

7. Hallquist, M.; Wenger, J. C.; Baltensperger, U.; Rudich, Y.; Simpson, D.; Claeys, M.; Dommen, J.; Donahue, N. M.; George, C.; Goldstein, A. H.; Hamilton, J. F.; Herrmann, H.; Hoffmann, T.; Iinuma, Y.; Jang, M.; Jenkin, M. E.; Jimenez, J. L.; Kiendler-Scharr, A.; Maenhaut, W.; McFiggans, G.; Mentel, T. F.; Monod, A.; Prévôt, A. S. H.; Seinfeld, J. H.; Surratt, J. D.; Szmigielski, R.; Wildt, J., The formation, properties and impact of secondary organic aerosol: current and emerging issues. *Atmos. Chem. Phys.* **2009,** *9*, (14), 5155-5236.

8. Crounse, J. D.; Nielsen, L. B.; Jørgensen, S.; Kjaergaard, H. G.; Wennberg, P. O., Autoxidation of organic compounds in the atmosphere. *The Journal of Physical Chemistry Letters* **2013,** *4*, (20), 3513-3520.

9. Mentel, T. F.; Springer, M.; Ehn, M.; Kleist, E.; Pullinen, I.; Kurtén, T.; Rissanen, M.; Wahner, A.; Wildt, J., Formation of highly oxidized multifunctional compounds: autoxidation of peroxy radicals formed in the ozonolysis of alkenes – deduced from structure–product relationships. *Atmos. Chem. Phys.* **2015,** *15*, (12), 6745-6765.

10. Bianchi, F.; Tröstl, J.; Junninen, H.; Frege, C.; Henne, S.; Hoyle, C. R.; Molteni, U.; Herrmann, E.; Adamov, A.; Bukowiecki, N.; Chen, X.; Duplissy, J.; Gysel, M.; Hutterli, M.; Kangasluoma, J.; Kontkanen, J.; Kürten, A.; Manninen, H. E.; Münch, S.; Peräkylä, O.; Petäjä, T.; Rondo, L.; Williamson, C.; Weingartner, E.; Curtius, J.; Worsnop, D. R.; Kulmala, M.; Dommen, J.; Baltensperger, U., New particle formation in the free troposphere: a question of chemistry and timing. *Science* **2016,** *352*, (6289), 1109-1112.

11. Ehn, M.; Thornton, J. A.; Kleist, E.; Sipila, M.; Junninen, H.; Pullinen, I.; Springer, M.; Rubach, F.; Tillmann, R.; Lee, B.; Lopez-Hilfiker, F.; Andres, S.; Acir, I. H.; Rissanen, M.; Jokinen, T.; Schobesberger, S.; Kangasluoma, J.; Kontkanen, J.; Nieminen, T.; Kurten, T.; Nielsen, L. B.; Jorgensen, S.; Kjaergaard, H. G.; Canagaratna, M.; Dal Maso, M.; Berndt, T.;

Petaja, T.; Wahner, A.; Kerminen, V. M.; Kulmala, M.; Worsnop, D. R.; Wildt, J.; Mentel, T. F., A large source of low-volatility secondary organic aerosol. *Nature* **2014,** *506*, (7489), 476.

12. Tröstl, J.; Chuang, W. K.; Gordon, H.; Heinritzi, M.; Yan, C.; Molteni, U.; Ahlm, L.; Frege, C.; Bianchi, F.; Wagner, R.; Simon, M.; Lehtipalo, K.; Williamson, C.; Craven, J. S.; Duplissy, J.; Adamov, A.; Almeida, J.; Bernhammer, A.-K.; Breitenlechner, M.; Brilke, S.; Dias, A.; Ehrhart, S.; Flagan, R. C.; Franchin, A.; Fuchs, C.; Guida, R.; Gysel, M.; Hansel, A.; Hoyle, C. R.; Jokinen, T.; Junninen, H.; Kangasluoma, J.; Keskinen, H.; Kim, J.; Krapf, M.; Kürten, A.; Laaksonen, A.; Lawler, M.; Leiminger, M.; Mathot, S.; Möhler, O.; Nieminen, T.; Onnela, A.; Petäjä, T.; Piel, F. M.; Miettinen, P.; Rissanen, M. P.; Rondo, L.; Sarnela, N.; Schobesberger, S.; Sengupta, K.; Sipilä, M.; Smith, J. N.; Steiner, G.; Tomè, A.; Virtanen, A.; Wagner, A. C.; Weingartner, E.; Wimmer, D.; Winkler, P. M.; Ye, P.; Carslaw, K. S.; Curtius, J.; Dommen, J.; Kirkby, J.; Kulmala, M.; Riipinen, I.; Worsnop, D. R.; Donahue, N. M.; Baltensperger, U., The role of low-volatility organic compounds in initial particle growth in the atmosphere. *Nature* **2016,** *533*, 527.

13. Richards-Henderson, N. K.; Goldstein, A. H.; Wilson, K. R., Large enhancement in the heterogeneous oxidation rate of organic aerosols by hydroxyl radicals in the presence of nitric oxide. *The Journal of Physical Chemistry Letters* **2015,** *6*, 4451-4455.

14. Richards-Henderson, N. K.; Goldstein, A. H.; Wilson, K. R., Sulfur dioxide accelerates the heterogeneous oxidation rate of organic aerosol by hydroxyl radicals. *Environmental Science and Technology* **2016,** *50*, 3554-3561.

15. Berkemeier, T.; Huisman, A. J.; Ammann, M.; Shiraiwa, M.; Koop, T.; Pöschl, U., Kinetic regimes and limiting cases of gas uptake and heterogeneous reactions in atmospheric aerosols and clouds: a general classification scheme. *Atmos. Chem. Phys.* **2013,** *13*, (14), 6663-6686.

16. Berkemeier, T.; Steimer, S. S.; Krieger, U. K.; Peter, T.; Poschl, U.; Ammann, M.; Shiraiwa, M., Ozone uptake on glassy, semi-solid and liquid organic matter and the role of reactive oxygen intermediates in atmospheric aerosol chemistry. *Physical Chemistry Chemical Physics* **2016,** *18*, (18), 12662-12674.

17. Davies, J.; Wilson, K., Nanoscale interfacial gradients formed by the reactive uptake of OH radicals onto viscous aerosol surfaces. *Chemical Science* **2015,** *6*, 7020-7027.

18. Houle, F. A.; Hinsberg, W. D.; Wilson, K. R., Oxidation of a model alkane aerosol by OH radical: the emergent nature of reactive uptake. *Phys. Chem. Chem. Phys.* **2015,** *17*, 4412-4423.

19. Houle, F. A.; Wiegel, A. A.; Wilson, K. R., Changes in reactivity as chemistry becomes confined to an interface. The case of free radical oxidation of C30H62 alkane by OH. *The Journal of Physical Chemistry Letters* **2018,** *9*, (5), 1053-1057.

20. Slade, J. H.; Knopf, D. A., Multiphase OH oxidation kinetics of organic aerosol: The role of particle phase state and relative humidity. *Geophysical Research Letters* **2014,** *41*, 5297-5306.

21. Slade, J. H.; Thalman, R.; Wang, J.; Knopf, D. A., Chemical aging of single and multicomponent biomass burning aerosol surrogate particles by OH: implications for cloud condensation nucleus activity. *Atmos Chem Phys* **2015,** *15*, 10183-10201.

22. Wiegel, A. A.; Liu, M. J.; Hinsberg, W. D.; Wilson, K. R.; Houle, F. A., Diffusive confinement of free radical intermediates in the OH radical oxidation of semisolid aerosols. *Physical Chemistry Chemical Physics* **2017,** *19*, (9), 6814-6830.

23. Wiegel, A. A.; Wilson, K. R.; Hinsberg, W. D.; Houle, F. A., Stochastic methods for aerosol chemistry: a compact molecular description of functionalization and fragmentation in the heterogeneous oxidation of squalane aerosol by OH radicals. *Phys. Chem. Chem. Phys.* **2015,** *17*, 4398-4411.

24. Che, D. L.; Smith, J. D.; Leone, S. R.; Ahmed, M.; Wilson, K. R., Quantifying the reactive uptake of OH by organic aerosols in a continuous flow stirred tank reactor. *Physical chemistry chemical physics : PCCP* **2009,** *11*, 7885-95.

25. Ware, W. R., Oxygen quenching of fluorescence in solution - an experimental study of diffusion process. *J Phys Chem-Us* **1962,** *66*, (3), 455.

26. Barrer, R. M.; Chio, H. T., Solution and diffusion of gases and vapors in silicone rubber membranes. *J Polym Sci Pol Sym* **1965**, (10pc), 111.

27

27. Moore, J. D.; Cui, S. T.; Cochran, H. D.; Cummings, P. T., Rheology of lubricant basestocks: A molecular dynamics study of C-30 isomers. *J Chem Phys* **2000,** *113*, (19), 8833-8840.

28. Hinsberg, W. D.; Houle, F. A. Kinetiscope: (http://hinsberg.net/kinetiscope/.

29. Wiegel, A. A.; Liu, M.; Hinsberg, W. D.; Wilson, K. R.; Houle, F. A., Diffusive confinement of free radical intermediates in the OH radical oxidation of semisolid aerosol. *Physical Chemistry Chemical Physics* **2017,** *19*, 6814-6830.

30. Zhang, Y.; Sanchez, M. S.; Douet, C.; Wang, Y.; Bateman, A. P.; Gong, Z.; Kuwata, M.; Renbaum-Wolff, L.; Sato, B. B.; Liu, P. F.; Bertram, A. K.; Geiger, F. M.; Martin, S. T., Changing shapes and implied viscosities of suspended submicron particles. *Atmos Chem Phys* **2015,** *15*, 7819-7829.

31. Lambe, A. T.; Ahern, A. T.; Williams, L. R.; Slowik, J. G.; Wong, J. P. S.; Abbatt, J. P. D.; Brune, W. H.; Ng, N. L.; Wright, J. P.; Croasdale, D. R.; Worsnop, D. R.; Davidovits, P.; Onasch, T. B., Characterization of aerosol photooxidation flow reactors: heterogeneous oxidation, secondary organic aerosol formation and cloud condensation nuclei activity measurements. *Atmospheric Measurement Techniques* **2011,** *4*, 445-461.

32. Kang, E.; Root, M. J.; Toohey, D. W.; Brune, W. H., Introducing the concept of Potential Aerosol Mass (PAM). *Atmos Chem Phys* **2007,** *7*, (22), 5727-5744.

33. Stone, D.; Whalley, L. K.; Heard, D. E., Tropospheric OH and HO2 radicals: field measurements and model comparisons. *Chem Soc Rev* **2012,** *41*, (19), 6348-6404.

34. Lelieveld, J.; Gromov, S.; Pozzer, A.; Taraborrelli, D., Global tropospheric hydroxyl distribution, budget and reactivity. *Atmos Chem Phys* **2016,** *16*, (19), 12477-12493.

35. Lee, L.; Wilson, K., The reactive–diffusive length of OH and ozone in model organic aerosols. *The Journal of Physical Chemistry A* **2016,** *120*, (34), 6800-6812.

36. Smith, J. D.; Kroll, J. H.; Cappa, C. D.; Che, D. L.; Liu, C. L.; Ahmed, M.; Leone, S. R.; Worsnop, D. R.; Wilson, K. R., The heterogeneous reaction of hydroxyl radicals with sub-micron

squalane particles: a model system for understanding the oxidative aging of ambient aerosols. *Atmos Chem Phys* **2009,** *9*, 3209-3222.

37. Ruehl, C. R.; Nah, T.; Isaacman, G.; Worton, D. R.; Chan, A. W. H.; Kolesar, K. R.; Cappa, C. D.; Goldstein, A. H.; Wilson, K. R., The influence of molecular structure and aerosol phase on the heterogeneous oxidation of normal and branched alkanes by OH. *The Journal of Physical Chemistry A* **2013,** *117*, 3990-4000.

38. Arangio, A. M.; Slade, J. H.; Berkemeier, T.; Pöschl, U.; Knopf, D. A.; Shiraiwa, M., Multiphase chemical kinetics of OH radical uptake by molecular organic markers of biomass burning aerosols: humidity and temperature dependence, surface reaction, and bulk diffusion. *The Journal of Physical Chemistry A* **2015,** *119*, 4533-4544.

39. Shiraiwa, M.; Li, Y.; Tsimpidi, A. P.; Karydis, V. A.; Berkemeier, T.; Pandis, S. N.; Lelieveld, J.; Koop, T.; Poschl, U., Global distribution of particle phase state in atmospheric secondary organic aerosols. *Nat Commun* **2017,** *8*, 15002.

40. Shiraiwa, M.; Ammann, M.; Koop, T.; Pöschl, U., Gas uptake and chemical aging of semisolid organic aerosol particles. *Proceedings of the National Academy of Sciences of the United States of America* **2011,** *108*, 11003-11008.

41. Pfrang, C.; Shiraiwa, M.; Pöschl, U., Chemical ageing and transformation of diffusivity in semi-solid multi-component organic aerosol particles. *Atmos. Chem. Phys.* **2011,** *11*, (14), 7343-7354.

42. Nah, T.; Kessler, S. H.; Daumit, K. E.; Kroll, J. H.; Leone, S. R.; Wilson, K. R., Influence of molecular structure and chemical functionality on the heterogeneous OH-initiated oxidation of unsaturated organic particles. *The journal of physical chemistry. A* **2014,** *118*, 4106-19.

43. Liu, M. J.; Wiegel, A. A.; Wilson, K. R.; Houle, F. A., Aerosol fragmentation driven by coupling of acid-base and free-radical chemistry in the heterogeneous oxidation of aqueous citric acid by OH radicals. *J Phys Chem A* **2017,** *121*, (31), 5856-5870.

29

555TOC graphic

556 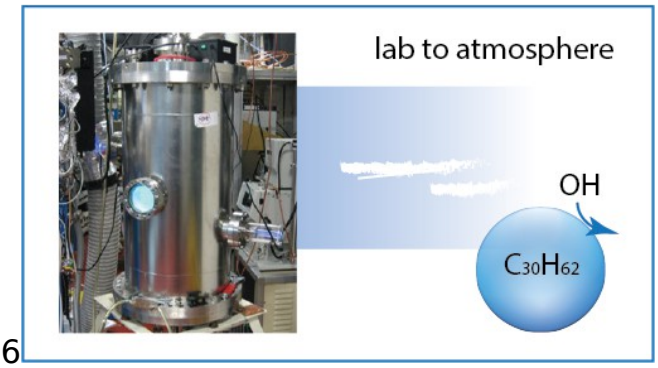

30